

Sensing performance enhancement via asymmetric gain optimization in the atom-light hybrid interferometer

ZHIFEI YU,¹ BO FANG,¹ PAN LIU,¹ SHUYING CHEN,¹ GUZHI BAO,²
CHUN-HUA YUAN,^{1,*} AND LIQING CHEN^{1,*}

¹State Key Laboratory of Precision Spectroscopy, Quantum Institute for Light and Atoms, Department of Physics, East China Normal University, Shanghai 200062, China

²School of Physics and Astronomy, and Tsung-Dao Lee Institute, Shanghai Jiao Tong University, Shanghai 200240, China

*chyuan@phy.ecnu.edu.cn

*lqchen@phy.ecnu.edu.cn

Abstract: The SU(1,1)-type atom-light hybrid interferometer (SALHI) is a kind of interferometer that is sensitive to both the optical phase and atomic phase. However, the loss has been an unavoidable problem in practical applications and greatly limits the use of interferometers. Visibility is an important parameter to evaluate the performance of interferometers. Here, we experimentally demonstrate the mitigating effect of the loss on visibility of the SALHI via asymmetric gain optimization, where the maximum threshold of loss to visibility close to 100% is increased. Furthermore, we theoretically find that the optimal condition for the largest visibility is the same as that for the enhancement of signal-to-noise ratio (SNR) to the best value with the existence of the losses using the intensity detection, indicating that visibility can act as an experimental operational criterion for SNR improvement in practical applications. Improvement of the interference visibility means achievement of SNR enhancement. Our results provide a significant foundation for practical application of the SALHI in radar and ranging measurements.

© 2022 Optical Society of America under the terms of the [OSA Open Access Publishing Agreement](#)

1. Introduction

Interferometers are widely used as sensors in precision measurement [1–4]. There have been many kinds of interferometers, such as optical interferometers [5–7], atom interferometers [8–13] and atom-light hybrid interferometer (ALHI) [14, 15]. Optical interferometers can measure the optical phase sensitive quantitation and are the core of optical gyroscopes [16], laser radar [17], ranging systems [18], etc. Atom interferometers can measure the atomic phase sensitive parameters, and have been demonstrated to measure the rotation rate [19], acceleration of gravity [20–22] and magnetic field [23, 24]. The ALHI is sensitive to both the optical and atomic phases, which has the potential to combine the advantages of optical wave and atomic systems in precision measurement, and has been utilized to measure angular velocity, electric field and magnetic field [14, 15, 25, 26].

In interferometry, the visibility represents the degree of interference cancellation of two beams, which can evaluate the performance of interferometers [12, 21, 27–29]. Low visibility has a negative effect on the measurement and causes a reduction in the SNR [28, 30, 31]. The SU(1, 1)-type interferometer realizes beam splitting and recombination through two parametric amplification processes [27, 32–34], whose two interference arms are quantum correlated. Comparing with conventional Mach-Zehnder interferometer (MZI), SNR of SU(1, 1)-type interferometer can break standard quantum limit due to quantum correlation. Previous literatures have shown that the SU(1, 1)-type interferometer has the tolerance to the detection loss (that is, external loss) by increasing the gain of the wave-recombination process [34–38]. However the SU(1, 1)-type interferometer, the internal loss has a greater effect on the perfect noise

cancellation between two beams [39, 40]. Noise cancellation is the advantage of the SU(1, 1)-type interferometer [41]. The internal loss limit the practical application of the SU(1, 1)-type interferometer in radar and ranging measurements. Recently, in the presence of internal losses, augmenting the visibility through asymmetry is shown in the all optical SU(1, 1) interferometer [42], and here we extend to the case of SALHI.

In this paper, we experimentally and theoretically investigate the visibility optimization of SU(1, 1)-type ALHI (SALHI) with the existence of the internal loss. The conventional MZI is also given as a comparison. The visibility of SALHI and MZI decreases with the loss. However, we theoretically give an optimization condition, under which the visibility of SALHI (V_{SU}) can be restored to $\sim 100\%$ by optimizing the gain factor of wave recombination process to satisfy the optimization condition over a wide range of internal loss. In experiment V_{SU} is restored to $\sim 90\%$. Furthermore, we theoretically analyze the SNR of the SALHI (SNR_{SU}) and find that the optimization condition for SNR_{SU} enhancement is the same as that for the visibility restoration, which implies that as long as the V_{SU} is improved, the SNR_{SU} can be enhanced. In experiment, it is difficult to judge whether the experimental conditions are suitable to achieve the best SNR_{SU} . However, the visibility is a physical quantity that is convenient to obtain and observe. Thus, the V_{SU} can be used as an experimental operational criterion for SNR_{SU} improvement. Therefore, the optimization condition and the V_{SU} restoration, have guiding significance for practical application of atom-light hybrid interferometers in the future.

2. SU(1, 1)-type atom-light hybrid interferometer

The scheme of the SALHI is shown in Fig. 1 (a), where two stimulated Raman scattering processes, SRS1 and SRS2, are used to realize the wave splitting and recombination of optical field and atomic spin wave. SRS1 generates \hat{a}_{s_1} and \hat{S}_{a_1} acting as two interference arms of SALHI, and then SRS2 is used to recombine \hat{a}'_{s_1} and \hat{S}'_{a_1} . The final interference outputs are optical signal \hat{a}_{s_2} and atomic spin wave \hat{S}_{a_2} , respectively.

When SRS is operated in single mode, which can be realized by using the seed \hat{a}_{s_0} and the W beam in spatial single-mode from single-mode fiber in experiment. The Hamiltonian of SRS can be written as [43]

$$\hat{H} = i\hbar\zeta A_W \hat{a}_s^\dagger \hat{S}_a^\dagger + H.c, \quad (1)$$

where $\zeta = (g_{eg}g_{em})/\Delta$, with g_{eg} , g_{em} are the coupling coefficients and Δ is the detuning frequency of the W field as Fig. 1 (a) shown. A_W is the amplitude of the strong W field. The input-output relationship of SRS1 is

$$\begin{aligned} \hat{a}_{s_1} &= G_1 \hat{a}_{s_0} + g_1 \hat{S}_{a_0}^\dagger, \\ \hat{S}_{a_1} &= G_1 \hat{S}_{a_0} + g_1 \hat{a}_{s_0}^\dagger, \end{aligned} \quad (2)$$

where \hat{a}_{s_0} and \hat{S}_{a_0} are the initially input states of the optical field and atomic spin wave, respectively. \hat{a}_{s_0} is the coherent state, and \hat{S}_{a_0} is the vacuum state. Between SRS1 and SRS2, a phase shift φ , internal loss l of the optical field, the dephasing η of the atomic spin wave are introduced. Then, \hat{a}_{s_1} becomes $\hat{a}'_{s_1} = \sqrt{1-l}\hat{a}_{s_1}e^{i\varphi} + \sqrt{l}\hat{v}$, and \hat{S}_{a_1} becomes $\hat{S}'_{a_1} = \sqrt{1-\eta}\hat{S}_{a_1} + \sqrt{\eta}\hat{F}$, where \hat{v} and \hat{F} are the operators of vacuum. After the SRS2 process, the interference outputs are

$$\begin{aligned} \hat{a}_{s_2} &= (G_1 G_2 \sqrt{1-l}e^{i\varphi} + g_1 g_2 \sqrt{1-\eta})\hat{a}_{s_0} + G_2 \sqrt{l}\hat{v} \\ &\quad + (G_2 g_1 \sqrt{1-l}e^{i\varphi} + G_1 g_2 \sqrt{1-\eta})\hat{S}_{a_0}^\dagger + g_2 \sqrt{\eta}\hat{F}^\dagger, \\ \hat{S}_{a_2} &= (G_1 g_2 \sqrt{1-l}e^{-i\varphi} + G_2 g_1 \sqrt{1-\eta})\hat{a}_{s_0}^\dagger + g_2 \sqrt{l}\hat{v}^\dagger \\ &\quad + (g_1 g_2 \sqrt{1-l}e^{-i\varphi} + G_1 G_2 \sqrt{1-\eta})\hat{S}_{a_0} + G_2 \sqrt{\eta}\hat{F}, \end{aligned} \quad (3)$$

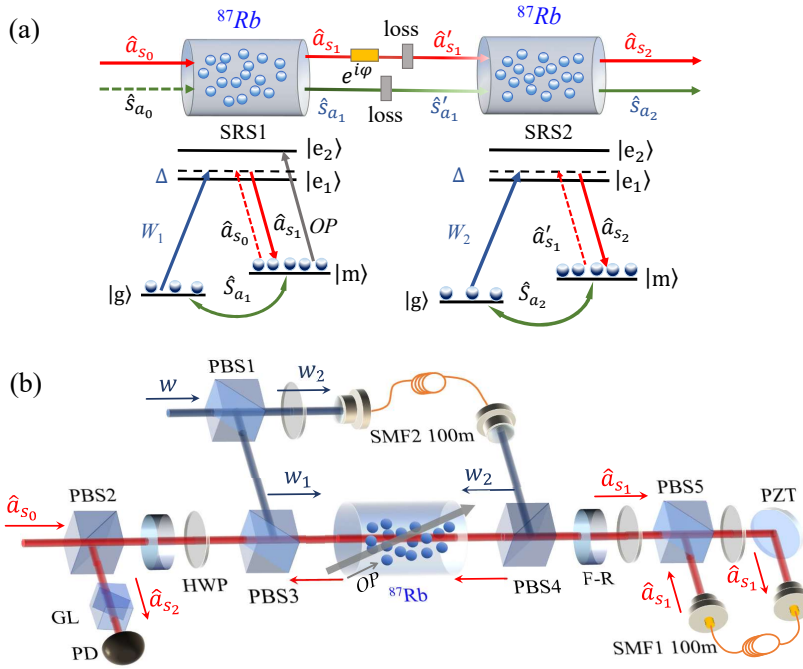


Fig. 1. (a) Scheme of the SALHI, energy level of the ^{87}Rb atom, and frequencies of the laser. \hat{a}_{s_0} and \hat{s}_{a_0} are the initially input optical field and atomic spin wave, respectively. \hat{a}_{s_1} and \hat{s}_{a_1} are the interference arms generated from SRS1, which then evolve to \hat{a}'_{s_1} and \hat{s}'_{a_1} after loss and phase shift φ , finally becoming interference outputs \hat{a}_{s_2} and \hat{s}_{a_2} after SRS2. SRS: stimulated Raman scattering. $|g, m\rangle$: $|5^2S_{1/2}, F = 1, F = 2\rangle$; $|e_1, e_2\rangle$: $|5^2P_{1/2}, F = 2\rangle$, $|5^2P_{3/2}\rangle$; W_1 and W_2 : Raman pump fields; OP: optical pumping field; Δ : single photon detuning. (b) Experimental setup of the SALHI. PZT: piezoelectric transducer; PBS: polarization beam splitter; HWP: half-wave plate; F-R: Faraday rotator; GL: Glan prism; SMF: single-mode fiber; PD: photon detector. The diameters of W_1 , W_2 and \hat{a}_{s_0} are all 0.5mm.

where the Raman gain factors $G_k = \frac{1}{2}(e^{\zeta_k A_W} + e^{-\zeta_k A_W})$ and $g_k = \frac{1}{2}(e^{\zeta_k A_W} - e^{-\zeta_k A_W})$ are related to A_W and Δ of the W field. $k = 1, 2$ represents SRS1 and SRS2, respectively. G_k and g_k satisfy $G_k^2 - g_k^2 = 1$. The outputs \hat{a}_{s_2} and \hat{s}_{a_2} both depend on the gain factors, the losses l , η and the phase shift.

3. Experimental setup

The experiment is performed in a cylindrical paraffin-coated ^{87}Rb vapor cell (diameter 0.5 cm, length 5 cm). As shown in Fig. 1(b), which was mounted inside a five-layer magnetic shield to reduce the stray magnetic field and heated to 75°C . Before the SRS1, almost all atoms are prepared in the ground state $|g\rangle$ by an optical pumping field (OP) resonant at the $|m\rangle \rightarrow |e_2\rangle$ transition. The OP pulse is $45 \mu\text{s}$ long, and its intensity is 110 mW. The W field is divided into W_1 and W_2 . W_2 is coupled into a 100 m-long single-mode fiber (SMF2). W_1 and initial input Stokes seed \hat{a}_{s_0} are spatially overlapped by PBS3 and interact the atoms via SRS1. The detuning frequency Δ of W is 1.2 GHz. The \hat{a}_{s_0} beam is red tuned 6.8 GHz from the W laser by an electro-optic modulator (EOM, Newport model No. 4851). After SRS1, \hat{s}_{a_1} stays in the cell. W_1 and \hat{a}_{s_1} exit the cell and are separated by PBS4. \hat{a}_{s_1} is coupled into 100 m-long SMF1 and then returned back into the atomic cell with the W_2 pulse to interfere with \hat{s}_{a_1} via SRS2. \hat{a}_{s_1} and

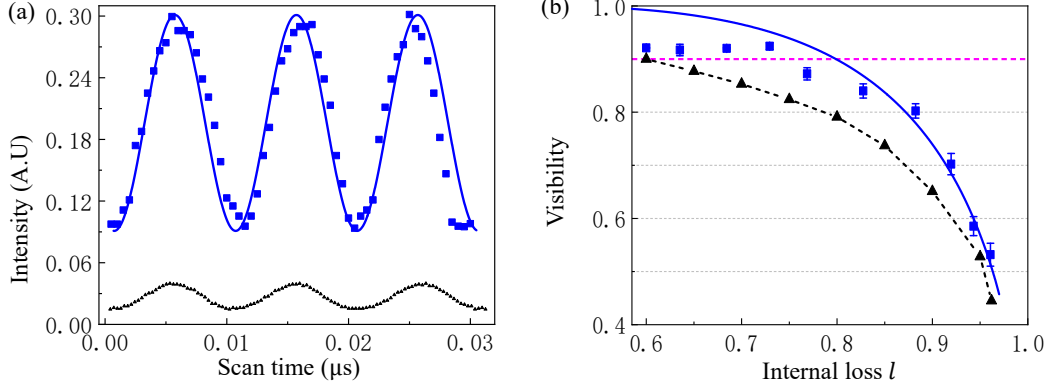


Fig. 2. (a) The blue squares are the interference fringes of the SALHI with fixed $G_1 = 3$, $G_2 = 5$, $l = 0.96$ and $\eta = 0.4$, and the black triangles are the interference fringes of the MZI under the same operating conditions. (b) The visibility value as a function of the loss rate l . The blue squares represent V_{SU} with fixed $G_1 = 3$, $G_2 = 5$ and $\eta = 0.4$, the blue solid curve is the result of theoretical fitting according to Eq. (4), and the black triangles are the values of V_{MZ} measured experimentally. The pink dashed line corresponds to a visibility of 90%.

W_2 are temporally and spatially overlapped. The phase shift φ of \hat{a}_{s_1} is controlled by the PZT. The optical interference output \hat{a}_{s_2} is detected by a photodetector after a Glan prism to filter W_2 . In experiment, the internal loss l of the optical interference beam is approximately 0.6, including the coupling efficiency of fiber, the transmittance of vapor cell and optical devices. The decay of the atomic spin wave is 0.4 due to atoms collisions and flying out of the interacting region during the evolution time between two SRS processes.

Comparing to optical MZI, whose two interference arms are both optical waves and the output is only sensitive to the optical phase, the SALHI goes one step further relying atom-photon correlation. Thus the interference fringes depends on both atomic and optical phases.

4. Visibility results

In the experiment, we first measured the V_{SU} and the visibility of MZI (V_{MZ}) with the same phase-sensitive particle number and internal loss as a comparison. Fig. 2 (a) shows the interference fringes of the Mach-Zehnder interferometer (MZI) and SALHI at $l=0.96$, $G_1 = 3$, $G_2 = 5$ and atomic decay rate $\eta = 0.4$ of \hat{S}_{a_1} . The values of the V_{MZ} and V_{SU} are 45 % and 53 %, respectively. Fig. 2 (b) shows the visibility value as a function of the loss rate l . In general, as the optical loss l of \hat{a}_{s_1} increases from 0.6 to 0.96 by variable attenuation plate, V_{SU} drops from 92.1% to 53%, and V_{MZ} is always smaller than V_{SU} under the same loss condition.

In theory, according to Eq. (3), the visibility of the optical interference output \hat{a}_{s_2} can be calculated and simplified as

$$V_{SU} \approx \frac{2G_1G_2g_1g_2\sqrt{1-l}\sqrt{1-\eta}}{G_1^2G_2^2(1-l) + g_1^2g_2^2(1-\eta)}. \quad (4)$$

V_{SU} depends not only on the gain factors (G_1, g_1, G_2, g_2) but also on the internal losses (η, l). The gain factors can be controlled by SRS parameters, such as the single-photon detuning Δ and power of W fields. We give the theoretical visibility values obtained by using corresponding experimental parameters ($G_1, g_1, G_2, g_2, \eta, l$) shown in fig. 2 (b) with blue solid lines. The theoretical predictions and experimental data match well.

5. Optimization condition

Furthermore, the largest interference visibility in Eq. (4) appears at

$$G_1 G_2 \sqrt{1-l} = g_1 g_2 \sqrt{1-\eta}. \quad (5)$$

We call this the optimization condition. According to Eqs. (2, 3), the interference output \hat{a}_{s_2} consists of two parts. One is $G_2 \hat{a}'_{s_1}$ amplified from the optical arm $\hat{a}'_{s_1} = \sqrt{1-l} \hat{a}_{s_1}$, and the other is $g_2 \hat{S}'_{a_1}$ amplified from the atomic arm $\hat{S}'_{a_1} = \sqrt{1-\eta} \hat{S}_{a_1}$. When the gain factor of the wave-recombination process (G_2) is adjusted to satisfy the $G_1 G_2 \sqrt{1-l} = g_1 g_2 \sqrt{1-\eta}$, the amplitudes of the two parts are equal, then the visibility of output \hat{a}_{s_2} can reach $\sim 100\%$.

The SNR is also an important parameter to characterize the performance of an interferometer and can be calculated by $\text{SNR} = \frac{[(\partial \langle \hat{O} \rangle / \partial \varphi) \delta]^2}{\langle (\Delta \hat{O})^2 \rangle}$ [44, 45], where \hat{O} is the measurable operator, δ is the added modulation small phase and $\langle (\Delta \hat{O})^2 \rangle = \langle \hat{O}^2 \rangle - \langle \hat{O} \rangle^2$. Under ID, the SNR_{SU} for the output optical field is

$$\text{SNR}_{\text{SU}} \approx \frac{4G_1^2 G_2^2 g_1^2 g_2^2 (1-l)(1-\eta) N_{\hat{a}_{s_0}} \sin^2 \varphi \delta^2}{A^2 (A^2 + B^2 + C^2)}, \quad (6)$$

where the input particle number $N_{\hat{a}_{s_0}} = \langle \hat{a}_{s_0}^+ \hat{a}_{s_0} \rangle$, $A^2 = G_1^2 G_2^2 (1-l) + g_1^2 g_2^2 (1-\eta) + 2G_1 G_2 g_1 g_2 \sqrt{1-l} \sqrt{1-\eta} \cos \varphi$, $B^2 = G_2^2 g_1^2 (1-l) + G_1^2 g_2^2 (1-\eta) + 2G_1 G_2 g_1 g_2 \sqrt{1-l} \sqrt{1-\eta} \cos \varphi$, and $C^2 = G_2^2 l + g_2^2 \eta$. SNR_{SU} is also related to internal losses (η, l) and gain factors (G_1, g_1, G_2, g_2). To find the best SNR_{SU} condition under a certain loss l , we calculate the partial derivative

$$\frac{\partial (\text{SNR}_{\text{SU}})}{\partial \sqrt{1-l}} = 0. \quad (7)$$

When the interferometer operates near the dark point, that is, $\varphi = \pi + \Delta\varphi$ and $\Delta\varphi \sim 0$, the solution of Eq. (7) is $G_1 G_2 \sqrt{1-l} = g_1 g_2 \sqrt{1-\eta}$, where the best SNR_{SU} can be achieved.

Obviously, this condition for the SNR_{SU} under ID is same as Eq. (5), indicating that the improvement of V_{SU} corresponds to enhancement of SNR_{SU} . The optimization condition is the key point to improve V_{SU} and enhance SNR_{SU} even at large internal loss. It should be noted that the interference visibility can be restored to $\sim 100\%$ and SNR_{SU} can be enhanced to the best value in the presence of losses when the experimental conditions satisfy the optimization condition. In the interferometer, phase shift can be measured using ID and balance homodyne detection (BHD). We also give the optimization condition for BHD in appendix part, which is different to Eq. (5).

To show the improvement of the SALHI compared with the conventional MZI under the same operating conditions, we calculated $\text{SNR}_{\text{MZ}} = \frac{(1-l)(1-\eta) N_0 \sin^2 \varphi \delta^2}{[(2-l-\eta) - 2\sqrt{1-l}\sqrt{1-\eta} \cos \varphi]}$ [46, 47],

where $N_0 = (2G_1^2 - 1) N_{\hat{a}_{s_0}}$ is the phase-sensitive particle number of the MZI. Figs. 3 (a-c) shows the visibility and Figs. 3 (d-f) shows the SNR as a function of the optical loss l . Firstly, before optimization, as the loss l increases, the SNR_{SU} first increase to a maximum value at $l = l_B$ and then decrease. In fact, l_B is the point satisfying the optimization condition $G_1 G_2 \sqrt{1-l} = g_1 g_2 \sqrt{1-\eta}$, and compared with MZI, the quantum interferometers has better visibility. However, Figs. 3 (d-f) shows that SNR_{SU} is larger than SNR_{MZ} only within a small l range near l_B under a certain G_1, G_2 and η , and as G_1 and η increase, this range is gradually diminished. The reason is that the increased G_1 or internal loss will bring more uncorrelated excess noise and quickly reduce the noise cancellation advantage of the SU(1, 1)-type interferometer. Therefore, when G_1, g_1 and η are fixed, finding a suitable G_2 satisfying

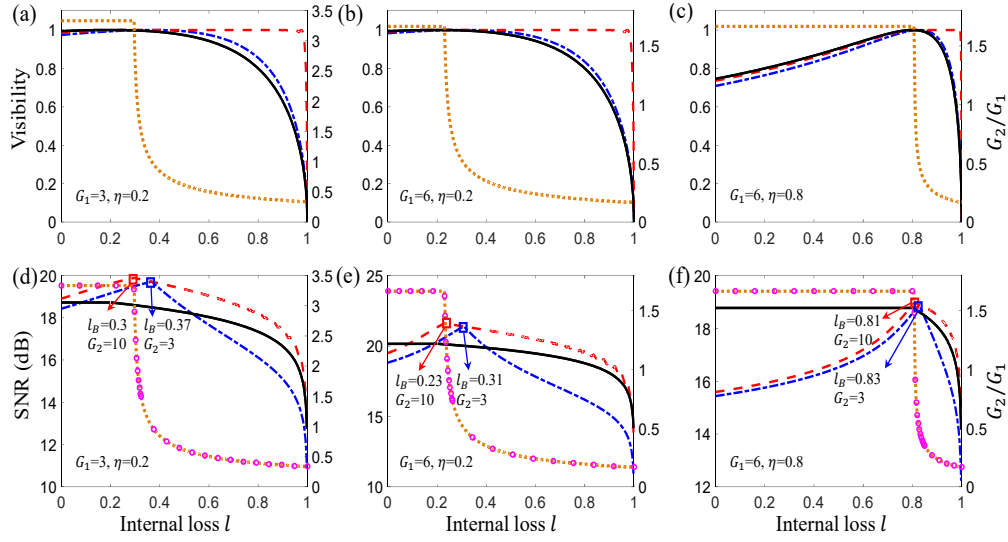


Fig. 3. (a-c) The V_{SU} before and after optimization of the output field \hat{a}_{s_2} and V_{MZ} as a function of l (left-hand vertical axis). The blue dash-dotted curve is V_{SU} before optimization with fixed gain factors G_1 , g_1 , G_2 , and g_2 . The red dashed curve is largest V_{SU} (right-hand vertical axis) after optimizing G_2 . The orange dotted curve is the value of G_2/G_1 after optimizing G_2 for the largest V_{SU} , the black solid line is V_{MZ} . (d-f) The black solid is SNR_{MZ} and the blue dash-dotted curves is SNR_{SU} before optimization with fixed gain factors G_1 , g_1 , G_2 , and g_2 , respectively, the red dashed curve is SNR_{SU} after optimizing G_2 (left-hand vertical axis). The pink circles represent the G_2/G_1 value at the best SNR_{SU} after optimization, and the orange dotted curve is the G_2/G_1 value of the largest V_{SU} after optimization (right-hand vertical axis).

the optimization condition at each l is an effective way to enhance $SNR_{SU} > SNR_{MZ}$ over a wider range of internal loss.

Fig. 3 also shows the optimal visibility and SNR_{SU} values (the left vertical axis) and corresponding G_2/G_1 value (the right vertical axis), G_2 is limited within 1~10 considering the experimental operability. First, V_{SU} and SNR_{SU} after optimization are larger than V_{MZ} and SNR_{MZ} over a wide range of losses. The optimized G_2 can effectively reduce the negative impact of the internal loss on V_{SU} and SNR_{SU} . Second, the optimized G_2 value is different in the regions of $l < l_B$ and $l > l_B$. For $l > l_B$, the optimal G_2 value is very small and can be directly calculated according to fixed G_1 , g_1 , η , and l . For $l < l_B$, we can not obtain the G_2 value completely satisfying the condition, only a larger G_2 value is closer to satisfying. Therefore as l increases, there is a common feature in Figs. 3 (a-c) that the optimized G_2/G_1 value first remains at the maximum value at $\leq l_B$ and then decrease sharply to a much smaller value at $l \geq l_B$. Finally, in Figs. 3 (d-f), the pink circles and the orange dotted curve completely coincide (the right vertical axis), showing that at any internal loss, the best SNR_{SU} corresponds to the point of largest V_{SU} . Optimization of V_{SU} is easy to observe in an experiment. As long as the maximum of V_{SU} is observed by optimizing G_2 , we can guarantee the best performance of the SU(1, 1)-type interferometer. This is different from the approach to compensate for the impact of the external loss.

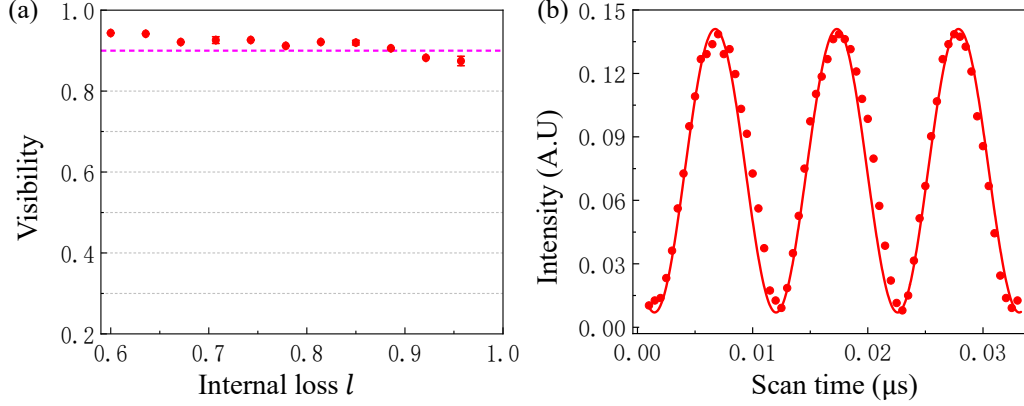


Fig. 4. (a) The red dots are the values of V_{opt} . The pink dashed line corresponds to a visibility of 90%. (b) The red dots are the interference fringes of the SALHI after optimization, corresponding to $G_2 \approx 1.3$ with $G_1=3$, $l=0.96$, and $\eta=0.4$, $V_{\text{opt}} = 88\%$.

6. Visibility restoration

Next, we provide an experimental demonstration of restoration of V_{SU} by optimizing G_2 in the SALHI. In practical applications such as radar or ranging measurement, when the parameters (G_1, g_1, η, l) are fixed, we can adjust only G_2 and g_2 to satisfy the optimization condition and improve the visibility. In the experiment, W_1 and W_2 are separated from the same laser as Fig. 1 (b) shown. Before the W_2 field enters the vapor cell, it passes through an attenuator and an AOM, which can be used to adjust the intensity and frequency of the W_2 field, respectively. Therefore, we can control G_2 by controlling the intensity and frequency of W_2 , so that the optimal condition is satisfied to obtain the best visibility. The experimental data of the visibility after optimizing G_2 (V_{opt}) are given in Fig. 4 (a) using red dots. V_{opt} is larger than the visibility without optimization (V_{SU}), and at $l = 0.6$, V_{opt} is 95%. As l increases, V_{opt} can remain at $\sim 90\%$ (see the pink dashed line), and the optimized G_2 is small at the loss l of 0.6-0.96 as in the theoretical prediction, such as $V_{\text{opt}}=88\%$ with $G_2 \approx 1.3$ when $l = 0.96$, and Fig. 4 (b) shows the interference fringes of the SALHI after optimization. The results show that the visibility can be restored even at large internal loss by optimizing G_2 , so the negative impact of internal loss on the properties of the SALHI can be mitigated. These experimental results are well consistent with the theoretical expectations.

7. Discussion and Conclusion

In conclusion, we have experimentally and theoretically researched the influence of the internal loss on the visibility of the SU(1, 1)-type ALHI. In general, the internal loss has a significant negative impact on the visibility. Moreover, we give the optimization condition $G_1 G_2 \sqrt{1-l} = g_1 g_2 \sqrt{1-\eta}$ for visibility restoration and experimentally demonstrate that the visibility can be restored to $\sim 90\%$ over a large range of internal loss by optimizing the G_2 factor to satisfy the optimization condition. Finally, we also theoretically find that the optimization condition for SNR_{SU} enhancement is the same as that for visibility restoration. Visibility as a physical quantity that is easy to obtain and observe, which can be used as an experimental operational criterion to judge whether the SNR_{SU} is optimized. What we have found will guide significance for practical application of quantum measurement.

8. APPENDIX: Comparison of optimization conditions of ID and BHD

1. The optimization conditions of seed light field \hat{a}_{s_0} input

After considering the losses l and η , the optimal condition for the best SNR_{SU} under the ID is $G_1 G_2 \sqrt{1-l} = g_1 g_2 \sqrt{1-\eta}$. Obviously, this corresponds to the condition of the largest visibility. However, under the BHD, the quadrature component of interference output at phase dark point $\varphi = 0$ is $\hat{X}_{\hat{a}_{s_2}}$,

$$\begin{aligned} \hat{X}_{\hat{a}_{s_2}} = & (G_1 G_2 \sqrt{1-l} + g_1 g_2 \sqrt{1-\eta}) \hat{a}_{s_0} + G_2 \sqrt{l} \hat{v} \\ & + (G_2 g_1 \sqrt{1-l} + G_1 g_2 \sqrt{1-\eta}) \hat{S}_{a_0}^\dagger + g_2 \sqrt{\eta} \hat{F}^\dagger \\ & + (G_1 G_2 \sqrt{1-l} + g_1 g_2 \sqrt{1-\eta}) \hat{a}_{s_0}^\dagger + G_2 \sqrt{l} \hat{v}^\dagger \\ & + (G_2 g_1 \sqrt{1-l} + G_1 g_2 \sqrt{1-\eta}) \hat{S}_{a_0} + g_2 \sqrt{\eta} \hat{F}, \end{aligned} \quad (8)$$

therefore, under the BHD,

$$\text{SNR}_{\text{SU}} = \frac{4(1-l)G_1^2 G_2^2 N_{\hat{a}_{s_0}} \delta^2}{\zeta_1^2 + \zeta_2^2 + \zeta_3^2}, \quad (9)$$

where $\zeta_1^2 = (G_1 G_2 \sqrt{1-l} + g_1 g_2 \sqrt{1-\eta})^2$, $\zeta_2^2 = (G_2 g_1 \sqrt{1-l} + G_1 g_2 \sqrt{1-\eta})^2$, $\zeta_3^2 = G_2^2 l + g_2^2 \eta$. We also calculate the partial derivative to find the optimization condition, the result is,

$$2\sqrt{1-l}\sqrt{1-\eta}G_1 G_2 g_1 g_2 = 2(1-\eta)g_1^2 g_2^2 + g_2^2 + G_2^2. \quad (10)$$

Obviously, this is different with the optimization condition of the largest visibility in Eq. (5).

2. The optimization conditions of initially prepared spin wave \hat{S}_{a_0}

From the Eq.(3), the visibility expression is:

$$V_{\text{SU}} \approx \frac{2G_1 G_2 g_1 g_2 \sqrt{1-l}\sqrt{1-\eta}}{G_2^2 g_1^2 (1-l) + G_1^2 g_2^2 (1-\eta)}. \quad (11)$$

Similarly, for largest visibility, the optimization condition is,

$$G_2 g_1 \sqrt{1-l} = G_1 g_2 \sqrt{1-\eta}. \quad (12)$$

Under the ID,

$$\text{SNR}_{\text{SU}} \approx \frac{4G_1^2 G_2^2 g_1^2 g_2^2 (1-l)(1-\eta) N_{\hat{a}_{s_0}} \sin^2 \varphi \delta^2}{B^2 (A^2 + B^2 + C^2)}, \quad (13)$$

from the Eq.(7) we can get the optimization condition of best SNR_{SU} is $G_2 g_1 \sqrt{1-l} = G_1 g_2 \sqrt{1-\eta}$, which is also same as optimization of largest visibility in Eq. (12).

However, under the BHD,

$$\text{SNR}_{\text{SU}} = \frac{4(1-l)G_2^2 g_1^2 N_{\hat{a}_{s_0}} \delta^2}{\zeta_1^2 + \zeta_2^2 + \zeta_3^2}, \quad (14)$$

the optimization condition of best SNR_{SU} is same as Eq. (10), which is also different with the optimization condition of largest visibility in Eq. (12).

In previous paper [14], we theoretically studied the SNR_{SU} using homodyne detection only considering optical loss l . In this paper, we further study the visibility and SNR_{SU} using ID and BHD with both losses l and η because these two losses are always exist simultaneously in practical application. We find that whether with optical input seed or initial atomic seed, the

optimization condition for best SNR_{SU} using ID is same as that of largest visibility, but different with that using BHD.

Therefore, here we experimentally measure the signal using ID. We can intuitively judge whether the optimization conditions for best SNR_{SU} is achieved according to the visibility restoration. And furthermore, compared with BHD, the ID device is simpler and more suitable for practical application of the SALHI in radar and ranging measurements.

Funding. This work was supported by the National Key Research and Development Program of China (2016YFA0302001); the National Natural Science Foundation of China (11874152, 11974111, 11654005, 91536114); the Shanghai Municipal Science and Technology Major Project (2019SHZDZX01); the innovation Program of Shanghai Municipal Education Commission (No. 202101070008E00099); the Fundamental Research Funds for the Central Universities; the Shanghai talent program and the Fellowship of China Postdoctoral Science Foundation (2020TQ0193).

Disclosures. The authors declare no conflicts of interest.

Data Availability . Data underlying the results presented in this paper are not publicly available at this time but may be obtained from the authors upon reasonable request.

References

1. X. Nie, J. Huang, Z. Li, W. Zheng, C. Lee, X. Peng, and J. Du, "Experimental demonstration of nonlinear quantum metrology with optimal quantum state." *Sci. Bull.* **63**, 469–476 (2018).
2. B. P. Abbott, R. Abbott, T. Abbott, F. Acernese, K. Ackley, C. Adams, T. Adams, P. Addesso, R. Adhikari, V. Adya *et al.*, "Gw170817: observation of gravitational waves from a binary neutron star inspiral," *Phys. Rev. Lett.* **119**, 161101 (2017).
3. L. S. Collaboration, V. Collaboration, M. Collaboration, D. E. C. G.-E. Collaboration, D. Collaboration, D. Collaboration, L. C. O. Collaboration, V. Collaboration, M. Collaboration *et al.*, "A gravitational-wave standard siren measurement of the hubble constant," *Nature* **551**, 85–88 (2017).
4. J. Liu, W. Liu, S. Li, D. Wei, H. Gao, and F. Li, "Enhancement of the angular rotation measurement sensitivity based on su (2) and su (1, 1) interferometers," *Photonics Res.* **5**, 617–622 (2017).
5. M. Xiao, L.-A. Wu, and H. J. Kimble, "Precision measurement beyond the shot-noise limit," *Phys. Rev. Lett.* **59**, 278 (1987).
6. R. S. Bondurant and J. H. Shapiro, "Squeezed states in phase-sensing interferometers," *Phys. Rev. D* **30**, 2548 (1984).
7. O. Steuernagel and S. Scheel, "Approaching the heisenberg limit with two-mode squeezed states," *J. Opt. B: Quantum Semiclassical Opt.* **6**, S66 (2004).
8. C. Gross, T. Zibold, E. Nicklas, J. Esteve, and M. K. Oberthaler, "Nonlinear atom interferometer surpasses classical precision limit," *Nature* **464**, 1165–1169 (2010).
9. Y.-J. Wang, D. Z. Anderson, V. M. Bright, E. A. Cornell, Q. Diot, T. Kishimoto, M. Prentiss, R. Saravanan, S. R. Segal, and S. Wu, "Atom michelson interferometer on a chip using a bose-einstein condensate," *Phys. Rev. Lett.* **94**, 090405 (2005).
10. M. Weitz, B. C. Young, and S. Chu, "Atomic interferometer based on adiabatic population transfer," *Phys. Rev. Lett.* **73**, 2563 (1994).
11. P. Hamilton, M. Jaffe, P. Haslinger, Q. Simmons, H. Müller, and J. Khoury, "Atom-interferometry constraints on dark energy," *Science* **349**, 849–851 (2015).
12. B. Estey, C. Yu, H. Müller, P.-C. Kuan, and S.-Y. Lan, "High-resolution atom interferometers with suppressed diffraction phases," *Phys. Rev. Lett.* **115**, 083002 (2015).
13. M. Kasevich and S. Chu, "Measurement of the gravitational acceleration of an atom with a light-pulse atom interferometer," *Appl. Phys. B* **54**, 321–332 (1992).
14. B. Chen, C. Qiu, S. Chen, J. Guo, L. Chen, Z. Ou, and W. Zhang, "Atom-light hybrid interferometer," *Phys. Rev. Lett.* **115**, 043602 (2015).
15. C. Qiu, S. Chen, L. Chen, B. Chen, J. Guo, Z. Ou, and W. Zhang, "Atom–light superposition oscillation and ramsay-like atom–light interferometer," *Optica* **3**, 775–780 (2016).
16. A. Matsko, A. Savchenkov, V. Ilchenko, and L. Maleki, "Optical gyroscope with whispering gallery mode optical cavities," *Opt. Commun.* **233**, 107–112 (2004).
17. P. A. Rosen, S. Hensley, I. R. Joughin, F. K. Li, S. N. Madsen, E. Rodriguez, and R. M. Goldstein, "Synthetic aperture radar interferometry," *Proc. IEEE* **88**, 333–382 (2000).
18. T. Kubota, M. Nara, and T. Yoshino, "Interferometer for measuring displacement and distance," *Opt. letters* **12**, 310–312 (1987).
19. T. Gustavson, P. Bouyer, and M. Kasevich, "Precision rotation measurements with an atom interferometer gyroscope," *Phys. Rev. Lett.* **78**, 2046 (1997).
20. A. Peters, K. Y. Chung, and S. Chu, "High-precision gravity measurements using atom interferometry," *Metrologia* **38**, 25 (2001).

21. P. Hamilton, M. Jaffe, J. M. Brown, L. Maisenbacher, B. Estey, and H. Müller, "Atom interferometry in an optical cavity," *Phys. Rev. Lett.* **114**, 100405 (2015).
22. X. Wu, Z. Pagel, B. S. Malek, T. H. Nguyen, F. Zi, D. S. Scheirer, and H. Müller, "Gravity surveys using a mobile atom interferometer," *Sci. advances* **5**, eaax0800 (2019).
23. M.-K. Zhou, Z.-K. Hu, X.-C. Duan, B.-L. Sun, J.-B. Zhao, and J. Luo, "Precisely mapping the magnetic field gradient in vacuum with an atom interferometer," *Phys. Rev. A* **82**, 061602 (2010).
24. C. F. Ockeloen, R. Schmied, M. F. Riedel, and P. Treutlein, "Quantum metrology with a scanning probe atom interferometer," *Phys. Rev. Lett.* **111**, 143001 (2013).
25. Y. Wu, J. Guo, X. Feng, L. Chen, C.-H. Yuan, and W. Zhang, "Atom-light hybrid quantum gyroscope," *Phys. Rev. Appl.* **14**, 064023 (2020).
26. S. Chen, L. Chen, Z.-Y. Ou, and W. Hang, "Quantum non-demolition measurement of photon number with atom-light interferometers," *Opt. express* **25**, 31827–31839 (2017).
27. F. Hudelist, J. Kong, C. Liu, J. Jing, Z. Ou, and W. Zhang, "Quantum metrology with parametric amplifier-based photon correlation interferometers," *Nat. communications* **5**, 1–6 (2014).
28. J. Kong, J. Jing, H. Wang, F. Hudelist, C. Liu, and W. Zhang, "Experimental investigation of the visibility dependence in a nonlinear interferometer using parametric amplifiers," *Appl. Phys. Lett.* **102**, 011130 (2013).
29. M. I. Kolobov, E. Giese, S. Lemieux, R. Fickler, and R. W. Boyd, "Controlling induced coherence for quantum imaging," *J. Opt.* **19**, 054003 (2017).
30. Z. Ou, "Enhancement of the phase-measurement sensitivity beyond the standard quantum limit by a nonlinear interferometer," *Phys. Rev. A* **85**, 023815 (2012).
31. M. Kacprowicz, R. Demkowicz-Dobrzański, W. Wasilewski, K. Banaszek, and I. Walmsley, "Experimental quantum-enhanced estimation of a lossy phase shift," *Nat. Photonics* **4**, 357–360 (2010).
32. B. Yurke, S. L. McCall, and J. R. Klauder, "Su (2) and su (1, 1) interferometers," *Phys. Rev. A* **33**, 4033 (1986).
33. K. Zheng, M. Mi, B. Wang, L. Xu, L. Hu, S. Liu, Y. Lou, J. Jing, and L. Zhang, "Quantum-enhanced stochastic phase estimation with the su (1, 1) interferometer," *Photonics Res.* **8**, 1653–1661 (2020).
34. Y. Liu, J. Li, L. Cui, N. Huo, S. M. Assad, X. Li, and Z. Ou, "Loss-tolerant quantum dense metrology with su (1, 1) interferometer," *Opt. Express* **26**, 27705–27715 (2018).
35. A. M. Marino, N. C. Trejo, and P. D. Lett, "Effect of losses on the performance of an su (1, 1) interferometer," *Phys. Rev. A* **86**, 023844 (2012).
36. M. Manceau, G. Leuchs, F. Khalili, and M. Chekhova, "Detection loss tolerant supersensitive phase measurement with an su (1, 1) interferometer," *Phys. Rev. Lett.* **119**, 223604 (2017).
37. E. Giese, S. Lemieux, M. Manceau, R. Fickler, and R. W. Boyd, "Phase sensitivity of gain-unbalanced nonlinear interferometers," *Phys. Rev. A* **96**, 053863 (2017).
38. M. Manceau, F. Khalili, and M. Chekhova, "Improving the phase super-sensitivity of squeezing-assisted interferometers by squeeze factor unbalancing," *New J. Phys.* **19**, 013014 (2017).
39. J. Xin, H. Wang, and J. Jing, "The effect of losses on the quantum-noise cancellation in the su (1, 1) interferometer," *Appl. Phys. Lett.* **109**, 051107 (2016).
40. W. Du, J. Chen, Z. Ou, and W. Zhang, "Quantum dense metrology by an su (2)-in-su (1, 1) nested interferometer," *Appl. Phys. Lett.* **117**, 024003 (2020).
41. D. Li, B. T. Gard, Y. Gao, C.-H. Yuan, W. Zhang, H. Lee, and J. P. Dowling, "Phase sensitivity at the heisenberg limit in an su (1, 1) interferometer via parity detection," *Phys. Rev. A* **94**, 063840 (2016).
42. Y. Michael, I. Jonas, L. Bello, M.-E. Meller, E. Cohen, M. Rosenbluh, and A. Pe'er, "Augmenting the sensing performance of entangled photon pairs through asymmetry," *Phys. Rev. Lett.* **127**, 173603 (2021).
43. K. Hammerer, A. S. Sørensen, and E. S. Polzik, "Quantum interface between light and atomic ensembles," *Rev. Mod. Phys.* **82**, 1041 (2010).
44. B. E. Anderson, P. Gupta, B. L. Schmittberger, T. Horrom, C. Hermann-Avigliano, K. M. Jones, and P. D. Lett, "Phase sensing beyond the standard quantum limit with a variation on the su (1, 1) interferometer," *Optica* **4**, 752–756 (2017).
45. Z.-D. Chen, C.-H. Yuan, H.-M. Ma, D. Li, L. Chen, Z. Ou, and W. Zhang, "Effects of losses in the atom-light hybrid su(1, 1) interferometer," *Opt. Express* **24**, 17766–17778 (2016).
46. R. Demkowicz-Dobrzanski, U. Dörner, B. Smith, J. Lundeen, W. Wasilewski, K. Banaszek, and I. Walmsley, "Quantum phase estimation with lossy interferometers," *Phys. Rev. A* **80**, 013825 (2009).
47. U. Dörner, R. Demkowicz-Dobrzanski, B. Smith, J. Lundeen, W. Wasilewski, K. Banaszek, and I. Walmsley, "Optimal quantum phase estimation," *Phys. Rev. Lett.* **102**, 040403 (2009).